10.24425/acs.2024.153102

Archives of Control Sciences
Volume 34(LXX), 2024
No. 4, *pages* 777–803

Geodesic path planning characteristics of the reconfigurable 1-S robot workspaces for hyperbolic, elliptical, and Euclidean geometries

Haydar SAHIN

The path-planning strategies are implemented by establishing the Riemann curvature tensor and geodesic equations of the 1-S robot workspace. This paper's originality lies in formulation of the parametric 1-S robot workspace for path planning, which is based on the differential geometry of the geodesic and Riemann curvature equations. The novel results in defining the path plan with diffeomorphic and expandable trajectories with zero and negative sectional curvatures are encouraging, as shown in the research article's result sections. The constant negative, constant positive, and zero sectional curvatures produce hyperbolic, elliptical, and Euclidean geometries. The workspace equation, derived using Lie algebra, defines the parameters of u_1, $_2$, u_3, and u_4 to obtain the shortest distances in path planning. The geodesic equations determine the shortest distances in the context of Riemann curvature tensor equations. These parameters from the workspace equation (α_1, α_2, θ_1, r_1) are used in the geodesic and Riemann curvature tensor equations. The results show that one needs to choose the most convenient parameters of the mechanism for path-planning capabilities. Both the topology of the mechanism, which is 1-S herein and the parameters of the workspaces should be selected for the pre-defined trajectories of the path planning, as shown in the results. The reconfigurable robots have many mechanism topologies to transform.

Key words: Riemann curvature tensor, geodesic equations, robot workspace, path planning, Dirac vector, Clifford algebra

1. Introduction

Differential geometry is a branch of mathematics that uses differentials to define geometrical motions with infinitesimal distances. Based on the differential

Author (e-mail: haydar.sahin@gedik.edu.tr) is with İstanbul Gedik University, Mechatronics Engineering, 34953 Kartal Türkiye.

This research did not receive any specific grant from funding agencies in the public, commercial, or not-for-profit sectors.

Received 3.8.2024. Revised 10.11.2024.

geometry of Riemann curvature and geodesic equations, this article defines and solves a parametric 1-S robot workspace. The diffeomorphic, that is differentiable spaces in C^{∞} are preferred for their applications in engineering. The diffeomorphic mapping for the manifolds involves differentiability, inverse mapping, and isomorphism [1]. Differential geometry definitions and theorems are modified and justified for 1-S robot workspaces.

Differentiability is critical to obtain the tangential T_pM spaces of the manifolds for structuring the surfaces. The mapping between the Riemann curvature tensor and the solutions of the geodesic equations is realized in this paper to specify the solved paths with their Riemann curvature tensors. The 1-S robot workspace requires the maneuverability of the generated path planning to pinpoint the actuators for joint motion. The Cartan-Hadamard theorem states that negative sectional curvature results in expandable manifold properties as well as diffeomorphisms in Euclidean space. Therefore, the Riemann curvature tensor is pivotal for the Riemann manifold. Sectional curvature can be derived using the Riemann curvature tensor. The Gauss curvature is a particular case of the sectional curvature concerning the two-dimensional surface [2]. Gauss discovered that the multiplication of the principal curvatures is intrinsic as a Gaussian curvature for the 2-manifold in R^3 [1]. The constant negative, positive, and zero sectional curvatures correspond to the hyperbolic, ellipsoid, and Euclidean flat geometries, respectively [1].

Lie groups, such as invertible square matrices, are smooth manifolds similar to the Riemann manifolds. The Riemann manifold is defined by the metric g and the differentiable manifold M by (M, g). Additionally, the Lie group is defined with tangential conversion via the Lie bracket of the Lie algebra for the exponential map. Meanwhile, the inner product of the Riemann metric as tangent space applies to any other manifolds along with the Riemann manifolds [3].

The local resemblance in R^n is capable of structuring the differential geometries contending with the points of space in order to establish the manifolds for various purposes. Spheres in S^2 space are examples of differentiable manifolds used in differential geometry literature to structure charts and atlases. Mapping of the manifolds of interest is required concerning the variously configured robot mechanisms and objects via charts and atlases. In the following sections, path planning is performed using the Riemann Curvature Tensor (RCT) and geodesic equations derived from the workspace equation for the 1-S robot [5]. The r_1 is the length of the Rigid Body (RB). 1-S robot mechanism of Fig. 1 is used to derive the spatial workspace Eqs. (1) and (2) [5]:

$$\xi^{S}_{0\_1\,j} = [0 \;\; 0 \;\; 0 \;\; \cos(\alpha_1)\cos(\alpha_2) - \cos(\alpha_2)\sin(\alpha_1)\sin(\alpha_2)]\,, \tag{1}$$

$$\mathrm{Ad}_{(g_{1\,j\_1})}\xi^{S}_{0\_1\,j}\,. \tag{2}$$

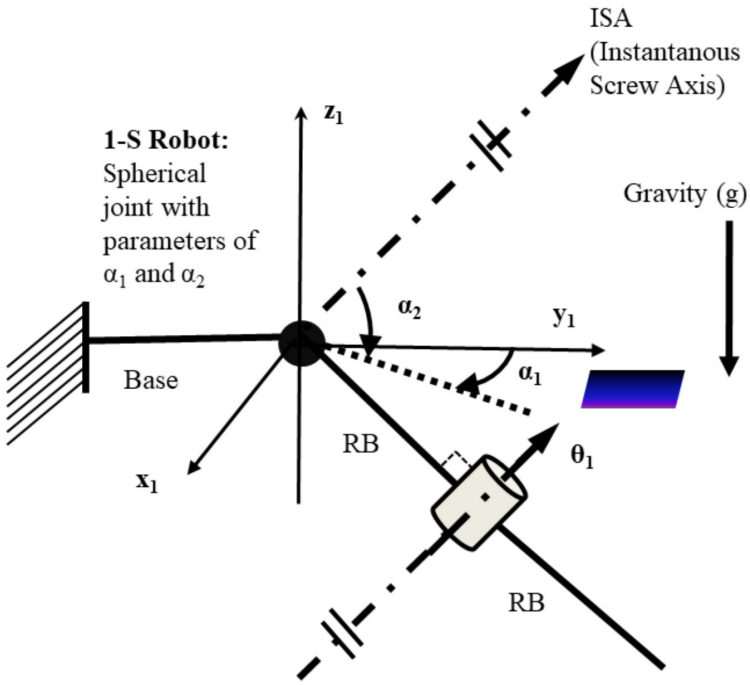

Figure 1: 1-S robot mechanism with the parameters α_1, α_2, θ_1, and r_1

Definition 1 (see [6])**.** [The workspace for 1-S robot]. *The Cartesian coordinate components x, y, z are defined as* $f_x(1,1)$, $f_y(2,1)$, $f_z(3,1)$ *in Eq. (3) where* α_1, α_2, θ_1 *and* r_1 *are the parameters of the Euclidean vector function. Herein, the workspace, f, was defined using Lie algebra as in Eq. (4). The Riemann curvature manifolds are defined using the workspace equation in x, y, and z coordinate to create the surface for the path planning purpose.*

The 1-S robot Riemannian manifolds were described using the $f(x, y, z)$ coordinates. The Riemannian structure can be defined using $f(x, y, z)$ for Riemannian sectional curvature. For path planning, it is convenient to define the manifold by the Riemann curvature tensor. The workspace of Eq. (2) was developed using Lie algebra [5]. Lie algebra, g, was developed using the adjoints for the revolute joint via the spatial workspace. Eqs. (1) and (2) are used to derive the spatial workspace equations using Lie algebra [5]. The 1-S robot workspace equation is derived using the Lie algebra of the $g^{-1}g$ (with the parameters α_1, α_2, θ_1, and r_1) [5].

After derivation of the workspace equation, the article herein can define the Riemann manifold parameters using it. These parameters are the manipulation and definition of the Riemannian sectional curvatures and geodesic equations.

Let $f_x,\ f_y,\ f_z$ be $x,\ y,\ z$ components of the cartesian coordinate of

$$\begin{aligned} f_x(1,1)(u_1,u_2,u_3u_4) &= (\alpha_1,\ \alpha_2,\ \theta_1,\ r_1),\\ f_y(2,1)(u_1,u_2,u_3u_4) &= (\alpha_1,\ \alpha_2,\ \theta_1,\ r_1),\\ f_z(3,1)(u_1,u_2,u_3u_4) &= (\alpha_1,\ \alpha_2,\ \theta_1,\ r_1), \end{aligned} \tag{3}$$

for the workspaces of the 1-S robot, as shown in Eq. (3).

Section 3 can derive the geodesic and Riemann curvature equations using the workspace Eq. (4). The selected two parameters, u, are for the Riemann sectional curvature and geodesic equations which structure the path planning of the 1-S robots.

$$f = \begin{pmatrix} \dfrac{r_1 \sin(2\alpha_1)\ \cos(\alpha_2)^2 \sin(\theta_1)}{2} + r_1 \sin(\alpha_2)\cos(\theta_1) \\ \dfrac{r_1\big(\cos(2\alpha_1)\cos(2\alpha_2) - \cos(2\alpha_2) + \cos(2\alpha_1) + 3\big)\sin(\theta_1)}{4} \\ [8pt] - r_1 \cos(\alpha_2)\big(\cos(\alpha_1)\cos(\theta_1) - \sin(\alpha_1)\sin(\alpha_2)\sin(\theta_1)\big) \end{pmatrix}. \tag{4}$$

The chart of the Riemann manifold, g, is used as the rank of two tensors for the tangent points of the defined surfaces from the 1-S robot workspaces. The 1-S robot workspace obtains the Riemann manifold for tangent points via (M, g) of g that is positive definite, symmetric, and nondegenerate [6].

Theorem 1. *[see [7], fundamental tensor of the workspace] The fundamental covariant 2-tensor field* $(0, 2)$ *determines the workspace, being positive definite, symmetric, and non-degenerate, along with the results for g from the 1-S robot workspaces, where g is symmetric with* $g_{12} = g_{21}$.

See the detailed proof of the Theorem 1 in [6]. This paper uses Einstein's summation convention [6]. The multiplication sign in the equation is defined for the tensors and vectors as declared in Eq. (5). One can see the positive definiteness of the g in Eq. (6), as stated in [6]:

$$\sum g_{ij} df^i \otimes df^j, \tag{5}$$

$$g_{ij} = g\left(\frac{\partial}{\partial f^i},\ \frac{\partial}{\partial f^j}\right). \tag{6}$$

2. Preliminaries and methodology

The Riemannian metric for g, defined as the inner product, is assigned to the smooth manifold of the Riemannian manifold M. Within the neighborhood of P, g_P is the tangent space metric of T_pM. The symmetric (0,2)-tensor field of

the g_{ij} structured smooth on the manifold for the tangent point P is the Riemann metric with positive definite characteristics for all the tangent points of P. The e_1, e_2 and e_3 vectors on the surface are eliminated in Eqs. (7) and (18) by using the Clifford algebra of the Cl $(3, 0, 1)$. When combined with the Lie algebra, the Dirac vector of the Clifford algebra is used for vector manipulation in a variety of contexts [8, 9]. The equations in Eqs. (8–(9) and Eq. (19) show such conversions for the geodesic equations and Riemann curvature tensor:

$$ds^2 = g_{ij} df^i df^j, \tag{7}$$

$$\gamma_k = e_j \frac{\partial f^j}{\partial u^k}. \tag{8}$$

The g fundamental covariant tensor $(0, 2)$ in S^2 for the Riemann manifold is derived using the directional Dirac vectors from Eq. (8) as in Eq. (9) [4, 10]

$$g_{jk} = (0.5)\left(\gamma_j \gamma_k + \gamma_k \gamma_j\right). \tag{9}$$

Eq. (10) shows another way to represent the Christoffel tensor [4, 10]

$$\Gamma^k_{ij} = g^{km} \Gamma_{mij}. \tag{10}$$

The nonlinear geodesic equations are represented with an indicial equation Eq. (11) using the Christoffel tensor [4, 10]

$$\frac{\partial^2 f^k}{\partial t^2} + \Gamma^k_{ij} \frac{\partial f^i}{\partial t} \frac{\partial f^j}{\partial t} = 0. \tag{11}$$

The Riemann curvature tensor equations represent the indicial notation of Eq. (12) using the Christoffel tensors and differential [4, 10]. The sectional curvature equations are derived by substituting the indices in the Riemann curvature Eq. (12)

$$R^i_{jkl} = \partial_k \Gamma^i_{lj} - \partial_l \Gamma^i_{kj} - \Gamma^m_{lj} \Gamma^i_{km} - \Gamma^m_{kj} \Gamma^i_{lm}. \tag{12}$$

The Riemann curvature tensor equations are converted into Gaussian curvatures with the indicial notation of equation in Eq. (13) after using the contravariant fundamental tensor [4, 10].

$$R = R^i_{kim} g^{km}. \tag{13}$$

The references are applied to validate and verify the calculations using the generalized Riemann curvature tensor and geodesic equations [4, 10]. The sectional curvatures can create Euclidean, Ellipsoid, or Hyperbolic trajectories, as shown in Fig. 2. Additionally, the isotropic path trajectories can be generated using the chosen sectional curvatures with geodesic solutions. Furthermore, the geodesic solutions in path planning can generate the shortest spatial distances, which is advantageous in optimization.

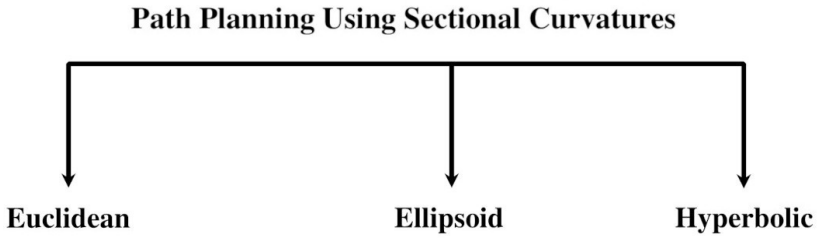

Figure 2: The path planning strategies for 1-S robot workspace via sectional curvature characteristics

3. Riemann curvature tensor and geodesics of the 1-S robot workspace

The derived equations using the formulations from the preliminaries section present the workspace of the 1-S robot in this section.

3.1. Workspace as manifold with Dirac vector of the Clifford algebra

The non-Euclidean space of the 1-S robot mechanism obtains the workspaces as a manifold for path planning in the Eq. (4) [5]. The x, y, and z coordinates are determined, as in Eq. (14). The multivector of geometric algebra called Clifford algebra integrates geometry with algebra, including the indicial notations of the tensors. Tensor algebra and vector spaces are mathematically processed and conducted using Clifford algebra. In a geometrical approach, the bivector, trivector, and multivector of the Clifford algebra have the potential for the tensor algebra. The scalar curvature is related to the Riemannian manifolds using the Dirac operator of the Clifford algebra [11, 12]. The Dirac vector is structured via the parameters u_1, u_2, u_3 and u_4. They can specify the affine structure without the specific coordinate system requirement. The Dirac vectors are orthogonal vectors for the specified surface structured via u_1, u_2, u_3 and u_4. The Riemann curvature tensor and geodesic equations confine with the aid of the Dirac vectors in the Clifford algebra of multi-vector algebra [10]

$$\begin{pmatrix} 0.005\sqrt{3}\sin(\alpha_2) + 0.0025\sin(\alpha_1)\cos(\alpha_2)^2 \\ 0.00125\big(\cos(2\alpha_1)\cos(2\alpha_2) - \cos(2\alpha_2) + \cos(2\alpha_1) + 3\big) \\ -0.01\cos(\alpha_2)\left(\dfrac{\sqrt{3}\cos(\alpha_1)}{2} - \dfrac{\sin(\alpha_1)\sin(\alpha_2)}{2}\right) \end{pmatrix} = \begin{pmatrix} f_x(\alpha_1, \alpha_2) \\ f_y(\alpha_1, \alpha_2) \\ f_z(\alpha_1, \alpha_2) \end{pmatrix}. \quad (14)$$

The parameters θ_1 and r_1 define u_1 and u_2. On the other hand, the substituted parameters are $u_3 = \alpha_1 = \dfrac{\pi}{6}$ and $u_4 = \alpha_2 = \dfrac{\pi}{6}$, as in Eq. (15)

$$\begin{pmatrix} \dfrac{3^{\frac{3}{2}} r_1 \sin(\theta_1)}{16} + \dfrac{r_1\cos(\theta_1)}{2} \\ \dfrac{13 r_1 \sin(\theta_1)}{16} \\ -\dfrac{\sqrt{3} r_1 \left(\dfrac{\sqrt{3}\cos(\theta_1)}{2} - \dfrac{\sin(\theta_1)}{4}\right)}{2} \end{pmatrix} = \begin{pmatrix} f_x(r_1, \theta_1) \\ f_y(r_1, \theta_1) \\ f_z(r_1, \theta_1) \end{pmatrix}. \quad (15)$$

Parameters θ_1 and α_2 are defined for u_1 and u_2. On the other hand, the substituted parameters are $u_3 = \alpha_1 = \dfrac{\pi}{3}$ and $u_4 = r_1 = 0.01$, as in Eq. (16)

$$\begin{pmatrix} 0.0025\sqrt{3}\sin(\alpha_2)^2\sin(\theta_1) + 0.01\sin(\alpha_2)\cos(\theta_1) \\ 0.0025\left(\dfrac{5}{2} + \dfrac{3\cos(\alpha_2)}{2}\right)\sin(\theta_1) \\ -0.01\cos(\alpha_2)\left(\dfrac{\cos(\theta_1)}{2} - \dfrac{\sqrt{3}\sin(\alpha_2)\sin(\theta_1)}{2}\right) \end{pmatrix} = \begin{pmatrix} f_x(\theta_1, \alpha_2) \\ f_y(\theta_1, \alpha_2) \\ f_z(\theta_1, \alpha_2) \end{pmatrix}. \quad (16)$$

Similarly, parameters of r_1 and α_2 are defined for u_1 and u_2. On the other hand, the substituted parameters are $u_3 = \alpha_1 = \dfrac{\pi}{6}$ and $u_4 = \theta_1 = \dfrac{\pi}{6}$, as in Eq. (17)

$$\begin{pmatrix} \dfrac{\sqrt{3} r_1 \sin(\alpha_2)}{2} + \dfrac{\sqrt{3} r_1 \cos(\alpha_2)^2}{8} \\ \dfrac{r_1\left(\dfrac{7}{2} - \dfrac{\cos(2\alpha_2)}{2}\right)}{8} \\ -r_1\cos(\alpha_2)\left(\dfrac{3}{4} - \dfrac{\sin(\alpha_2)}{4}\right) \end{pmatrix} = \begin{pmatrix} f_x(r_1, \alpha_2) \\ f_x(r_1, \alpha_2) \\ f_z(r_1, \alpha_2) \end{pmatrix}. \quad (17)$$

The trivector, bivector, vector, and scalar are some of the components of the multivector Clifford algebra, with a rank of three, two, one, and zero, respectively.

Clifford algebra's Dirac vectors, also known as geometrical algebra, are derived from the Riemann metric equation's ds invariant displacement. The Riemann metric's g_{ij} covariant tensor is a fundamental symmetric tensor with rank two.

The geodesic equations use the Killing vectors on the Riemann manifold to solve for peculiar sectional curvatures [13]. The workspaces of the robot mechanism define the task spaces in the nonflat and non-Euclidean geometry therein. The deviation from parallel transport can be measured using the Riemann curvature tensor [10]. The algebraic metric tensor, the multivector algebra of the Clifford algebra, is utilized to derive the Riemann curvature tensor

$$\begin{aligned}\gamma_2 = {} & r_1\Big(\hat{e}_3\big(\cos(\alpha_1)\cos(\theta_1) - \sin(\alpha_1)\sin(\alpha_2)\sin(\theta_1)\big)\sin(\alpha_2)\Big) \\ & + r_1\sin(\theta_1)\left(\hat{e}_3\sin(\alpha_1)\cos(\alpha_2)^2\right) \\ & + \frac{r_1\sin(\theta_1)\Big(2\left(\hat{e}_2\sin(2\alpha_2)\right) - 2\big(\hat{e}_2\cos(2\alpha_1)\sin(2\alpha_2)\big)\Big)}{4} \\ & - r_1\sin(\theta_1)\big(\hat{e}_1\sin(2\alpha_1)\cos(\alpha_2)\sin(\alpha_2)\big) + r_1\cos(\theta_1)\big(\hat{e}_1\cos(\alpha_2)\big), \quad (18)\end{aligned}$$

$$g_{22} = 0.25\begin{pmatrix}\begin{pmatrix} r_1^2\sin(2\alpha_1)^2\cos(2\alpha_2)^2 + 4r_1^2\cos(2\alpha_1)^2\cos(\alpha_2)^4 \\ + r_1^2\sin(2\alpha_1)^2 \end{pmatrix}\sin(\theta_1)^2 \\ +8r_1^2\cos(\alpha_1)\sin(\alpha_1)\cos(\alpha_2)^2\sin(\alpha_2)\cos(\theta_1) + \sin(\theta_1) \\ + 4r_1^2\sin(\alpha_1)^2\cos(\alpha_2)^2\cos(\theta_1)^2 \end{pmatrix}. \quad (19)$$

Parameter γ_j in Eq. (8) [10] can be analyzed first. The unitary e_i vectors are eliminated in the g_{ij} equations as in Eq. (19), which exist in the Dirac vector equation as in Eq. (19). Because g_{ij} is the metric tensor of the Riemann manifold, the vectors e_i are no longer required. The algebraic tensor can use the Cl $(3, 0, 1)$ matrix as the coordinate system to manipulate the inner products. The Dirac vector of the Clifford algebra is defined as Cl $(3, 0, 1)$ [10], as shown in Eq. (6).

3.2. Geodesic differential equations for workspaces

The selected two parameters, from α_1, α_2, θ_1, and r_1, are among those in the 1-S workspace equations. The equations solve these two substituted parameters. The u_1 and u_2 are the selected parameters to solve in the geodesic equations, while the u_3 and u_4 are constant values substituted in the geodesic and workspace equations. Upon establishing the Riemann manifolds via M and g, the geodesic equations solve the workspace equations for the path planning with the sectional curvatures determined.

The variable u_x is defined as $\dfrac{u_1}{u_2}$ to be solved using the Runge-Kutta (RK) numerical algorithm. RK is used to solve nonlinear geodesic differential equa-

tions. The various two parameters of the workspace are operated to analyze the geodesic path planning. These parameters are shown in Table 1 with the selected scenarios.

3.3. The Riemann curvature tensor of the workspace

The Riemann curvature tensor Eq. (12) is utilized to derive the sectional curvature equation Eq. (13). The sectional curvatures of R1121, R1212, R1112, and R1221, as solved for various scenarios in Table 1, are determined by the Riemannian manifolds specified by the parameters.

The spatial surface of the Riemannian manifold is formed by the solutions of the geodesic equations and the Riemann curvature tensor. As a result, the path planning was constrained by the results of the diffeomorphic Riemann curvature tensors chosen.

4. Results

The selected u_1 and u_2 parameters from the 1-S robot workspace are shown in Table 1. The results of the 1-S robot workspace equations are functions of the sines and cosines, as shown in equations (14) and (15). The diffeomorphic characteristic of the sinusoidal functions for the mentioned equations makes the results of the workspaces convenient for path planning. Additionally, the covariant tensor field $(0, 2)$ of g for defined (M, g) Riemann manifolds is smooth topological manifolds [6] concerning the workspaces.

Table 1: Selected parameters for u with scenarios of 1-S robot workspace to solve in geodesic differential equations for path planning

Selected	Parameters as Scenarios					
u_1 and u_2	$\alpha_1,\ \alpha_2$	$\alpha_1,\ r_1$	$\alpha_1,\ \theta_1$	$\alpha_2,\ r_1$	$\alpha_2,\ \theta_1$	$\theta_1,\ r_1$
u_3 and u_4	$r_1,\ \theta_1$	$\theta_1,\ \alpha_2$	$r_1,\ \alpha_2$	$\theta_1,\ \alpha_1$	$\alpha_1,\ r_1$	$\alpha_1,\ \alpha_2$

The topological manifold points of M satisfy Hausdorff, homeomorphic, and second countability. Herein, these satisfied points are generated from the workspace equations. These covariant tensor fields of $(0, 2)$ with g are generated from Dirac vectors, as shown in Eq. (18). The Clifford algebra $\mathrm{Cl}\,(3, 0, 1)$ creates the differentiable topological manifolds of the (M, g) Riemann manifolds. Herein, the Dirac vectors of the Clifford algebra are generated from the workspace equation of the 1-S robot [5, 14, 15]. The u_3 and u_4 parameters are arranged to create various path-planning strategies. The objective herein is to classify the manifolds created by the selected parameters u_1 and u_2 using the workspace generated by

the Lie algebra. This novel classification is closing the gap in the literature for the 1-S robot workspace of the created paths via the Riemann manifolds with geodesic equations.

Cartan Hadamard Theorem states the negative sectional curvature causes the diffeomorphism in Euclidean space. This diffeomorphism can be seen in the results section herein. Though various scenarios are tested in Table 1, only the majority of scenarios in Table 2 are revealed in the results section due to space limitations.

Table 2: Selected parameter *values* for u_3 and u_4 with scenarios of 1-S robot workspace to solve in geodesic differential equations for path planning

Selected u_3 and u_4 parameter values											
r_1	θ_1	θ_1	α_2	r_1	α_2	θ_1	α_1	α_1	r_1	α_1	α_2
0.01	0.005π	$\pi/6$	π	0.01	$\pi/10$	$\pi/6$	π	$\pi/3$	0.01	$\pi/6$	$\pi/4$
0.01	0.00π	$\pi/6$	$\pi/4$	0.01	$\pi/2.5$	$\pi/6$	$\pi/4$			$\pi/3$	$\pi/3$
0.01	$\pi/2$	$\pi/3$	$\pi/3$			$\pi/3$	$\pi/3$				
0.01	$\pi/3$										
0.01	$\pi/6$										

The shortest distance on the defined surface is derived using the geodesic differential equations of the variables' initial conditions. The regional categories of the 1-S robot workspace path trajectories classify negative and positive sectional curvatures. The results, as shown in Table 2, are arranged according to the regions 1, 2, 3, and 4 of the Riemann sectional curvatures. The methods for isotropic geometry and symmetrical and nonsymmetrical geometries are defined using the Riemann sectional curvatures in regions 1, 2, 3, and 4. The defined regions are for the sectional curvature region shown in Tables 2 and 3.

Table 3: Selected regions for R1121, R1121, R1221, R1212, and R1112 with parameters of 1-S robot workspace to solve in geodesic differential equations for path planning

REGIONS	CONSTRAINT EQUATIONS OF THE SECTIONAL CURVATURES
Region one	$-100000 < R < -5$
Region two	$-5 < R < 50000$
Region three	$50000 < R < 1000000$
Region four	The remaining: $R > 100000$ & $R < -100000$

5. Discussions

In the literature, geodesic trajectory planning relied on generalized algorithms derived from geodesic equations rather than in-depth analyses based on parametric workspace equations, as completed herein. The novelty of this paper in path planning is that the geodesic and Riemann curvature tensor equation results are analyzed concurrently and systematically using the parameters α_1, α_2, θ_1, and r_1 of the derived 1-S robot workspace [5]. The parametric integration of the geodesic and Riemann curvature tensors in analyses is also a novel approach for the 1-S robot workspace with the parameters α_1, α_2, θ_1, and r_1. This article adds to the literature the value of parametric analyses of the path planning strategies using the geodesic and Riemann curvature tensors with the derived workspace of the 1-S robots [5].

5.1. The parameters α_1 and α_2

Geodesic path planning is established by generating the 1-S robot workspace parameters α_1 and α_2, which define the sinusoidal diffeomorphic surfaces. The numerical solution for α_1 and α_2 is derived from the nonlinear geodesic differential equations associated with the 1-S robot workspace equations. For the θ_1 value of zero, the paths remain in the vertical plane of the $z - x$ axis as in Fig. 3a. In Fig. 3b, the distinguished paths are generated by varying θ_1 on a small scale in the direction of the y-axis. The nonlinear geodesic differential equations have solutions for $u_1 = \alpha_2$, $u_2 = \alpha_1$, $r_1 = 0.01$, and $\theta_1 = 0.005\pi$. The workspace equation, substituted into Eq. (14), is one of the derived nonlinear geodesic differential equations from the workspace equations of the 1-S robot [5]. Workspace equations for 1-S robots show $u_2 = \alpha_1$ equations varying from 0 to 6 radians and $u_1 = \alpha_2$ equations varying from 0 to −90 radians. In Fig. 3c, the solution of the nonlinear geodesic differential equations for $\theta_1 = \dfrac{\pi}{6}$ generates the shortest path plan for the range of $\alpha_1 = 0{-}6$ radians.

The parametric variations of Eq. (19) for path planning are for α_1 and α_2. The workspaces are for the various sectional curvatures, as shown in Fig. 4a. The characteristic of the paths yields continuous circular geodesic paths. The geodesic equation, with large areas, can generate the route in various spatial circular directions, as shown in Fig. 4b for the $\theta_1 = \dfrac{\pi}{2}$. The characteristic of the path is unique compared to the rest of the surfaces' manifold. The characteristic of the trajectory, a spider-like shape, can be defined as spreading from one point to the spatial geodesic paths circularly.

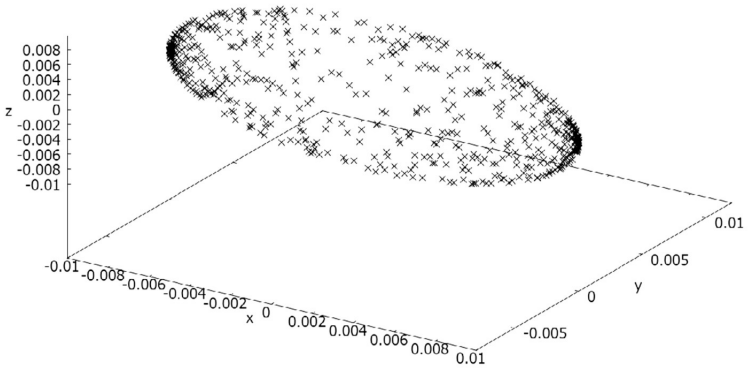

(a) $r_1 = 0.01$ and $\theta_1 = 0.00\pi$

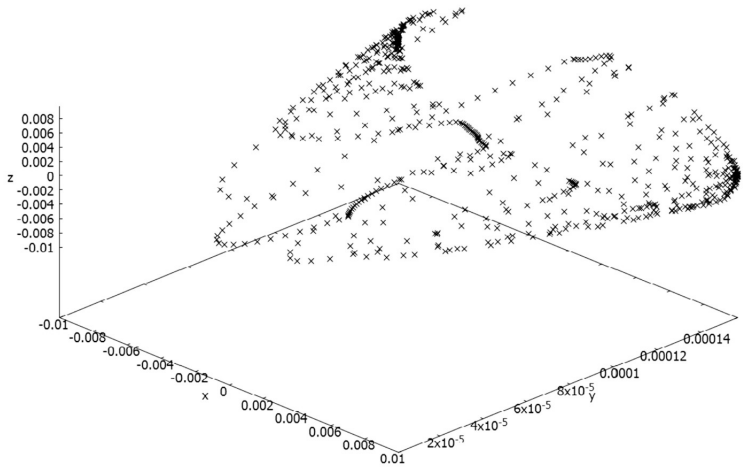

(b) $r_1 = 0.01$ and $\theta_1 = 0.005\pi$

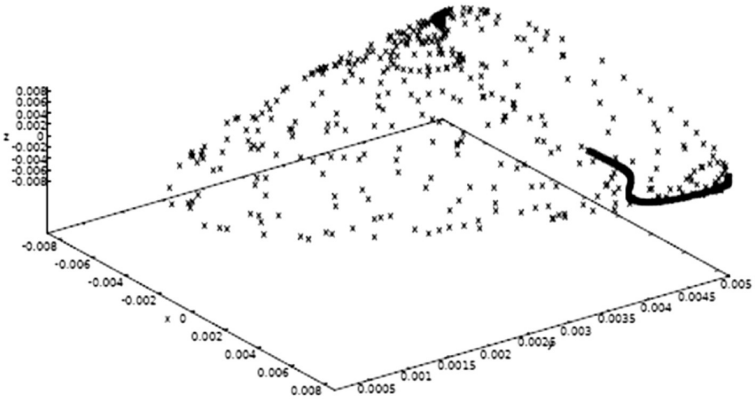

(c) $r_1 = 0.01$ and $\theta_1 = \pi/6$

Figure 3: The solution of the nonlinear geodesic differential equations for $u_1 = \alpha_2$, $u_2 = \alpha_1$, $r_1 = 0.01$

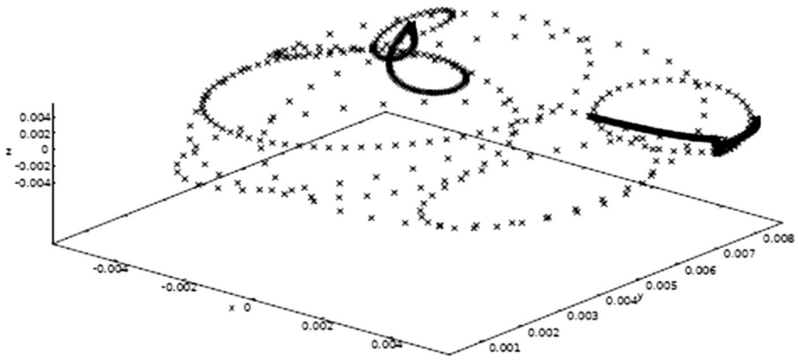

(a) $r_1 = 0.01$ and $\theta_1 = \pi/3$

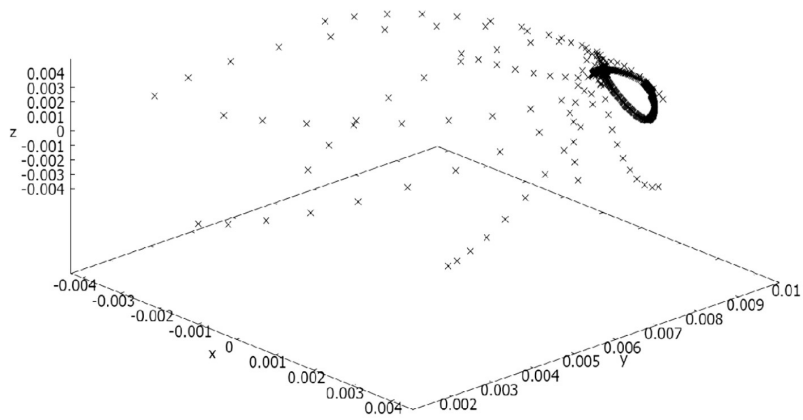

(b) $r_1 = 0.01$ and $\theta_1 = \pi/2$

Figure 4: The solution of the nonlinear geodesic differential equations for $u_1 = \alpha_2$, $u_2 = \alpha_1$ as the path trajectories in x, y and z coordinates

5.2. The parameters θ_1 and α_2

The results concern R1112, R1212, R1221, and R1121 of all sectional curvatures. They are composed of negative, zero, and positive values, as in Fig. 5a. The negative sectional curvatures for R1212, values between -50000 and 5, cause the diffusion of the path trajectories, as shown in Fig. 5b and 6a. This situation is addressed by Gauss-Bonnett theorem [1]. The convergent sectional curvatures of -5 to 50000 structure the path trajectories in certain directions, as seen in Fig. 5c and 6b for the positive sectional curvature values of the Gauss-Bonnet theorem. The remaining sectional curvature values are shown for the R1212 in Fig. 5d and 6c.

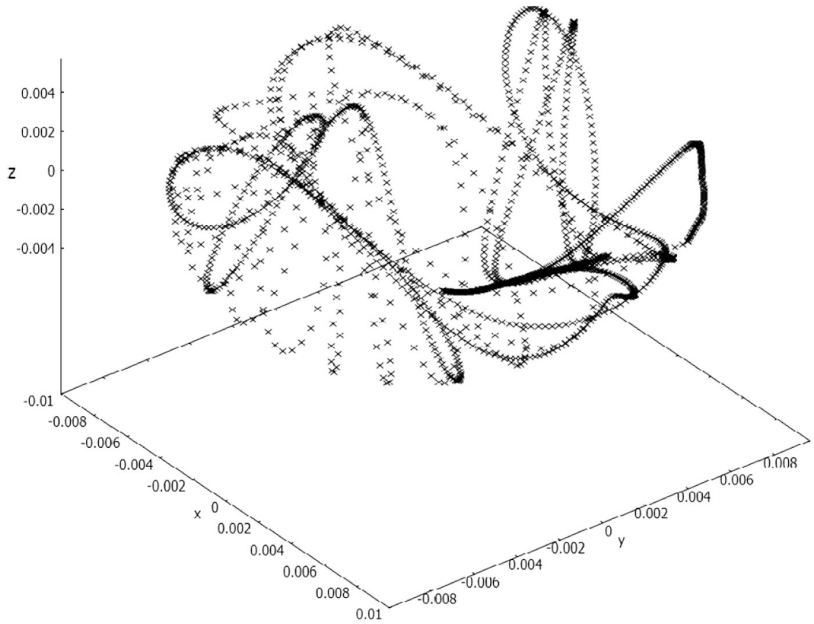

(a) All of the points for $r_1 = 0.01$ and $\alpha_1 = \pi/3$ scenarios

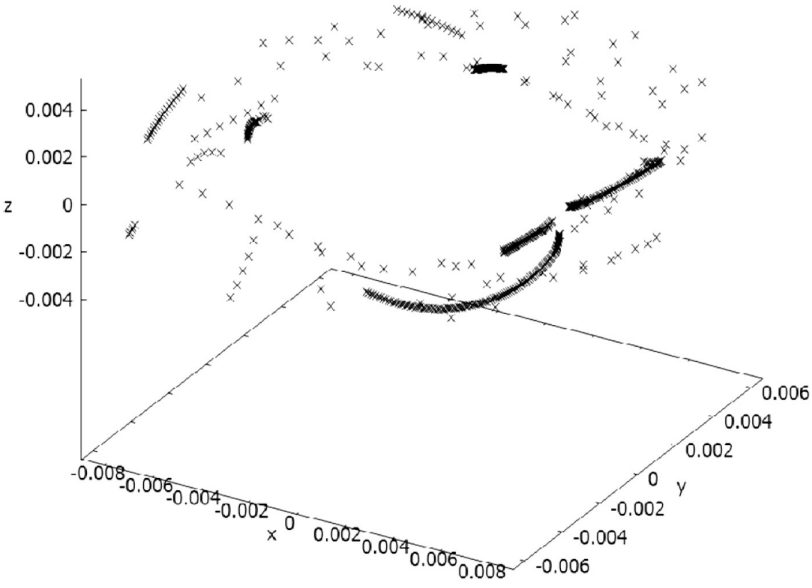

(b) The sectional curvature R1212 of the −50000 to 5

Figure 5

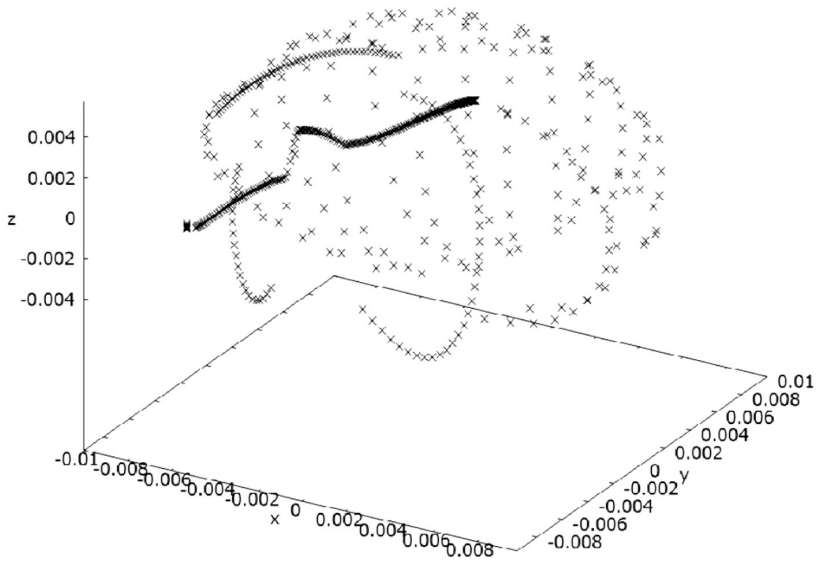

(c) For R1212 of the −5 to 50000

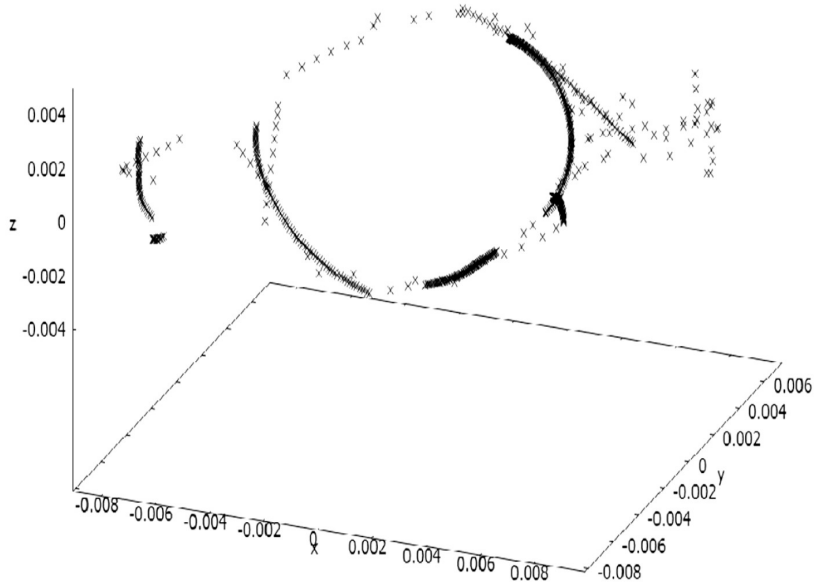

(d) For R1212 of the remaining sectional curvatures

Figure 5: The θ_1 and α_2 results of $r_1 = 0.01$ and $\theta_1 = \pi/3$

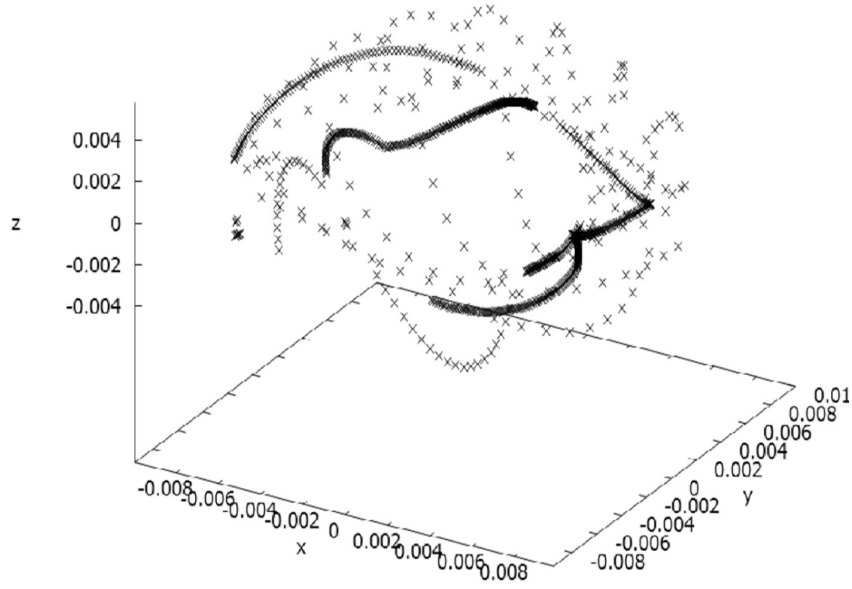

(a) R1121 of the −50000 to 5

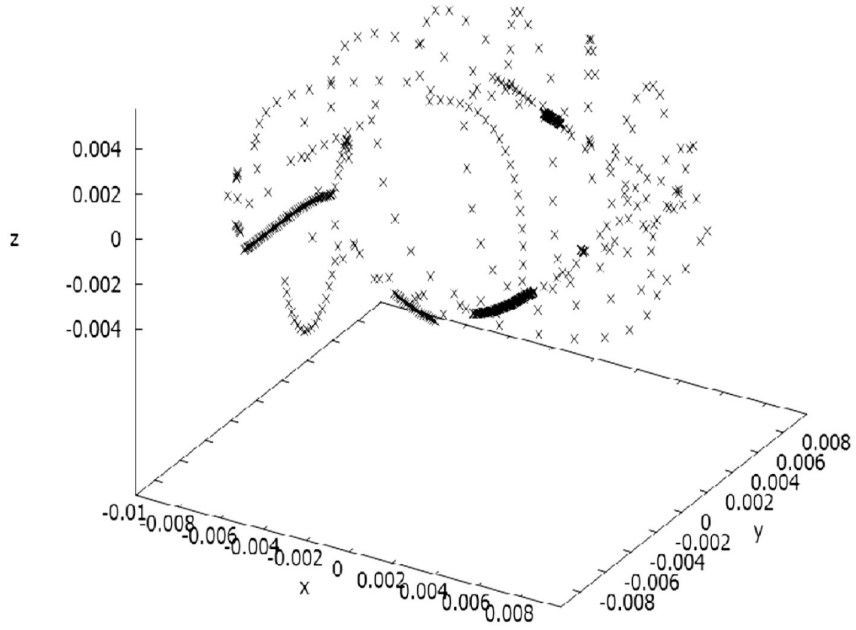

(b) R1121 of the −5 to 50000

Figure 6

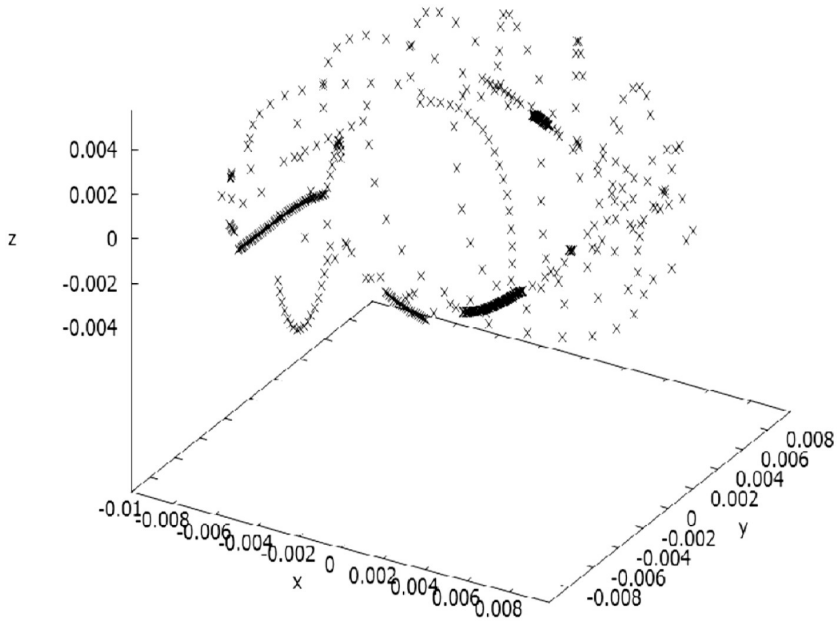

(c) The remaining high curvatures

Figure 6: The θ_1 and the α_2 results $r_1 = 0.01$ and $\theta_1 = \pi/3$ for R1121

5.3. The parameters θ_1 and r_1

The geodesic path characteristic, shown in Fig. 7a, is almost on a flat surface, which is consistent with the sectional curvature results shown in Figs. 7b and 7c for $\alpha_1 = \pi/3$. The results are nearly flat for the geodesic path parameters θ_1 and r_1. The low sectional curvature values are similar to the manifold of almost flat manifold surfaces. Because curvature is the reciprocal of radius, the curvature for almost flat trajectory is very high. As the result, low curvature implies a large radius of curvature. Furthermore, small sectional curvature values cause maneuverability with a large radius of curvature. This type of radius of curvature causes low spatial maneuverability capability since the traversing for the generated track is close to the flat road.

As shown in Fig. 7b and 7c, the sectional curvatures of R1212 and R1121 are in the range of 0.01–0. All the remaining sectional curvatures are zeros. The non-zero values only for the R1212 and R1121 sectional curvatures in Figs. 7b and 7c cause the rotational path trajectory shapes on almost flat surfaces, as shown in Fig. 7a. Additionally, the values of these only non-zero curvatures are small. Since these nonzero curvatures are only in the range of 10^{-3}, this results in generating trajectories on flat surfaces, resembling Euclidean space.

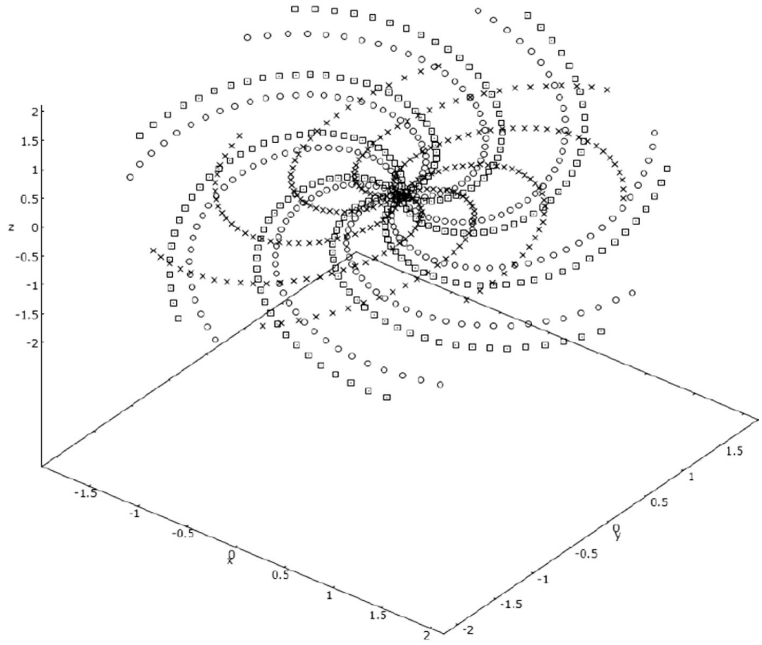

(a) The trajectories of the points

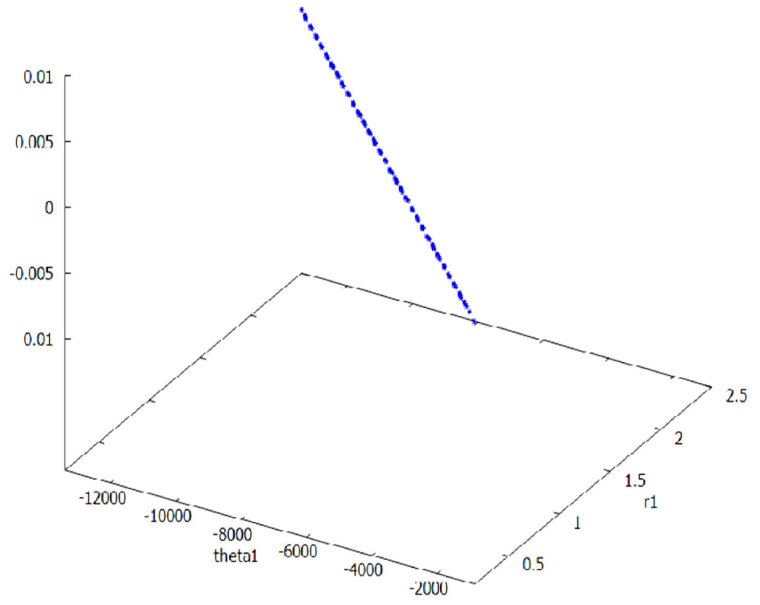

(b) Sectional curvature of R1121

Figure 7

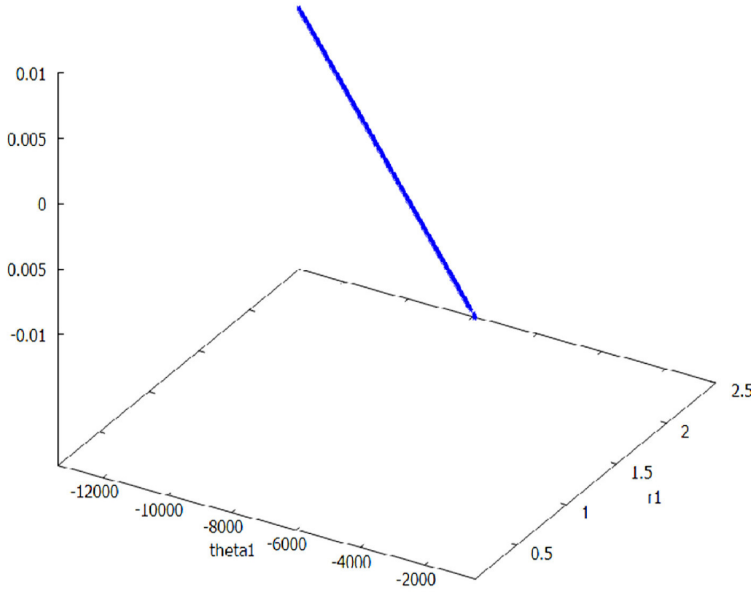

(c) Sectional curvature of R1212

Figure 7: The solution of the nonlinear geodesic differential equations for the workspaces of the $u_1 = \theta_1$, $u_2 = r_1$, $\alpha_1 = \pi/6$ and $\alpha_2 = \pi$ for multiply sign. $u_1 = \theta_1$, $u_2 = r_1$, $\alpha_1 = \pi/6$ and $\alpha_2 = \pi/4$ for square sign. The solution of the $\alpha_1 = \pi/3$ and $\alpha_2 = \pi/3$ for legend of circle

5.4. The parameters α_1 and r_1

The sectional curvatures of the R1121 and R1112 are so small that they are close to zero, as illustrated in Figs. 9a, 9b. The sectional curvatures of the R1121 are close to zero values for the path trajectories in Fig. 9a. The result shows the converging paths in Fig. 9. The curvatures are mostly either negative or close to zero values towards specific directions.

The positive curvature of the R1221 is in the lateral direction, as seen in Fig. 9c, which states the constant positive curvatures. R1212, as shown in Fig. 9e, has the only positive curvature that varies in the vertical direction. Thus, it is inevitable to generate the converging trajectory, as seen in Fig. 8, according to the mentioned theorems. The characteristics of the nonlinear workspace equations determine the trajectories' inclination for the selected variables of the α_1 and r_1 of the 1-S robot workspace. Therefore, trajectories can be designed using the selected parameters for workspaces. Because R1112's sectional curvatures are close to zero, the path trajectories converge in Fig. 9b. The result shows the converging paths in Fig. 8. The distinct path trajectory is created in Fig. 8 for the R1221 sectional curvature, as seen in Fig. 9c.

The negative diffusing, spreading diffeomorphic characteristics are shown in the R1212 sectional curvature of Fig. 9d. Since the highest negative sectional curvature exists for the R1212, the diffeomorphism with diffusion occurs in this direction of the Riemann curvature tensor. The trajectories of Fig. 8 can verify this trend rising in the same direction upward.

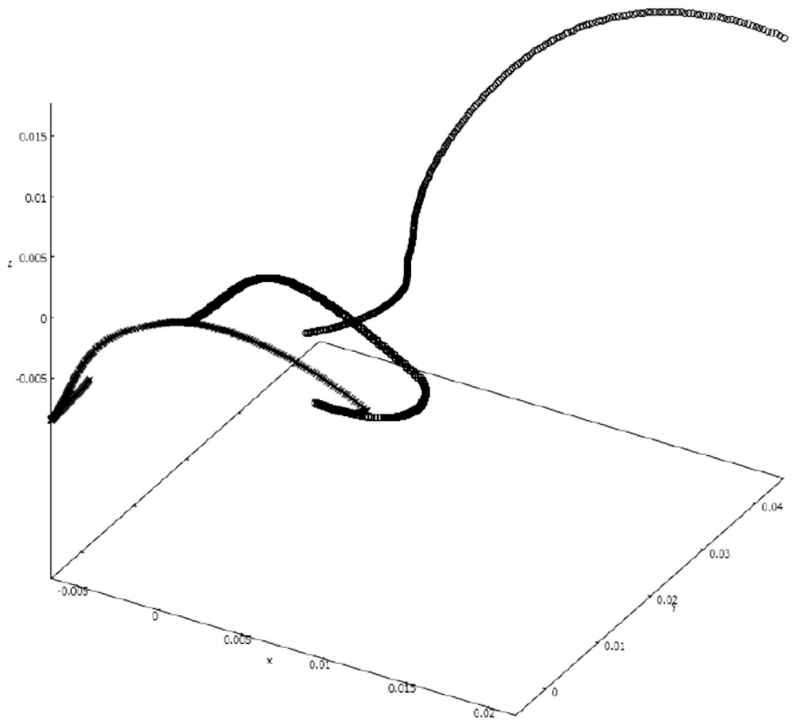

Figure 8: The solution of the nonlinear geodesic differential equations for the $u_1 = \alpha_1$, $u_2 = r_1$, multiply sign $\alpha_2 = \pi$ and $\theta_1 = \pi/6$; square sign $\alpha_2 = \pi/4$, and $\theta_1 = \pi/6$; circle sign $\theta_1 = \pi/3$, and $\alpha_2 = \pi/3$

Figure 9f shows that the low quantity of the highest values of the sectional curvatures for R1212 results in less maneuverability. The reduction in maneuverability is also evident in Fig. 8, which shows a distinct path trajectory in a specific direction. Since the R1212's sectional curvature range is significantly wider than the rest, it will dominantly determine the trajectory inclinations. Therefore, only one type of sectional curvature is majorly active in designing the path trajectories, which will generate a clear and specific line-type trajectory. This situation makes the path trajectories in a spatially sequential as towards to the unique line like direction.

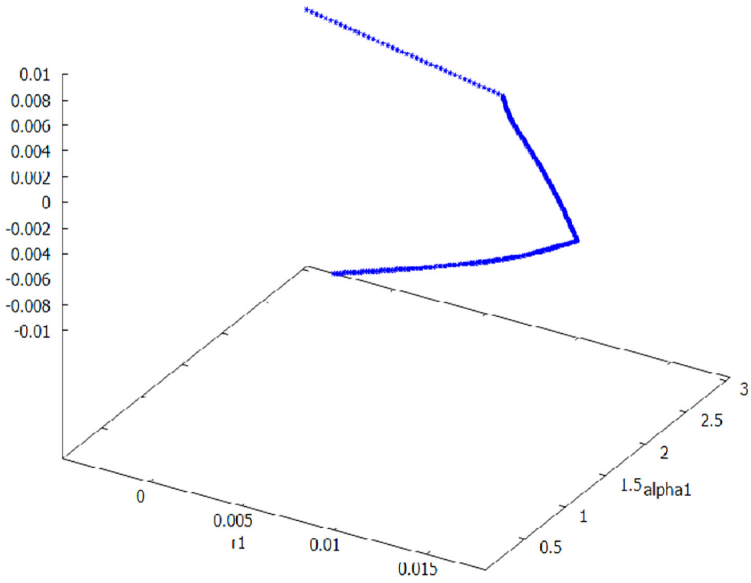

(a) R1121

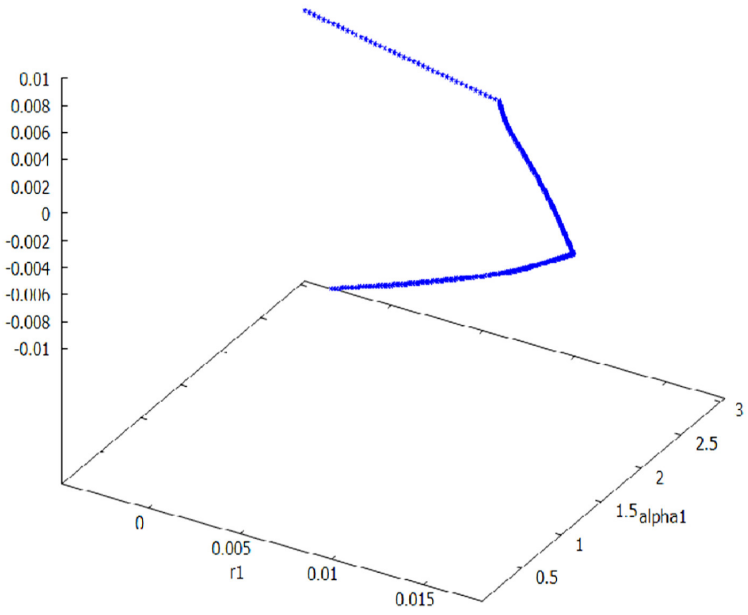

(b) R1112

Figure 9

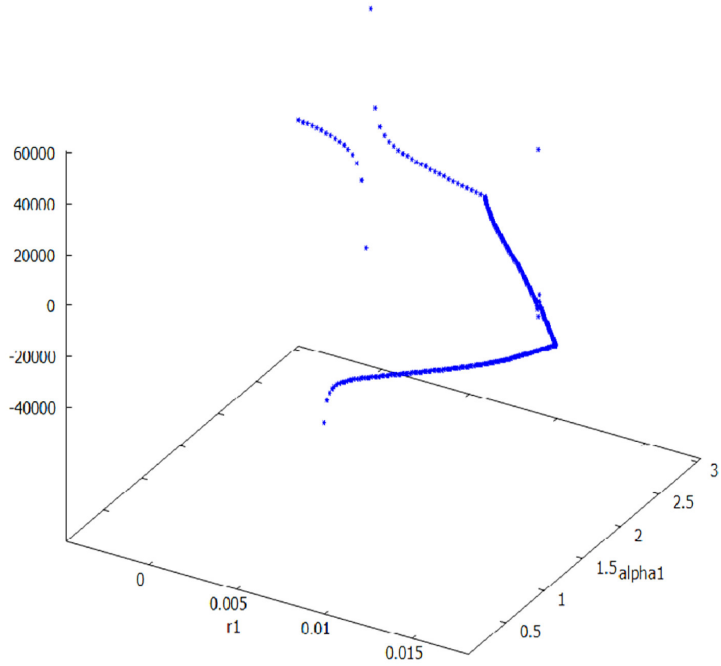

(c) R1221

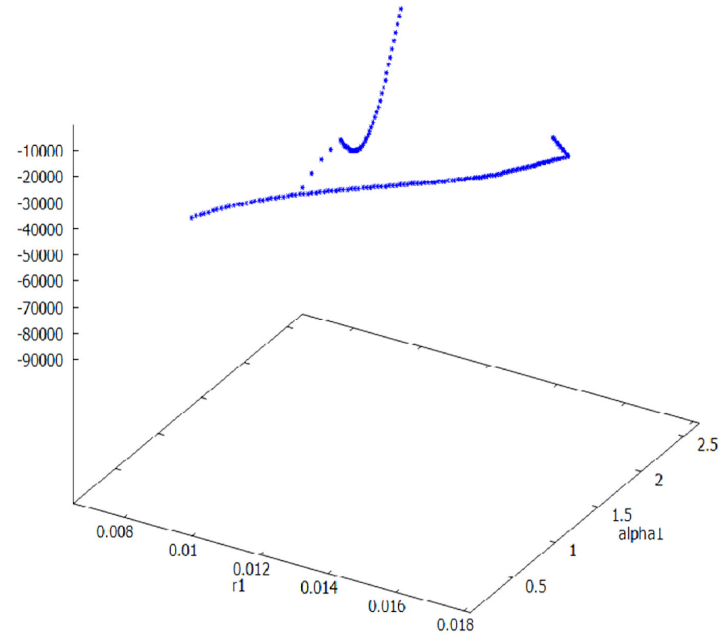

(d) $-100000 < R1212 < -5$

Figure 9

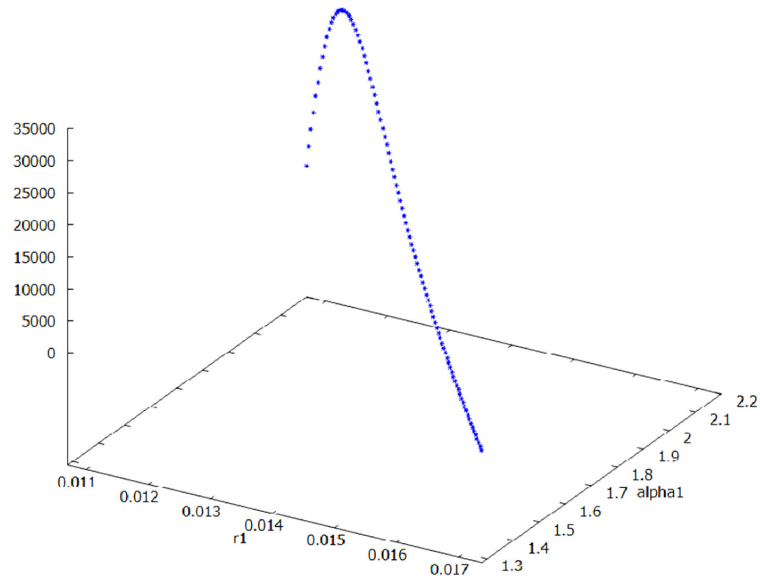

(e) $5 \leqslant$ R1212 < 50000

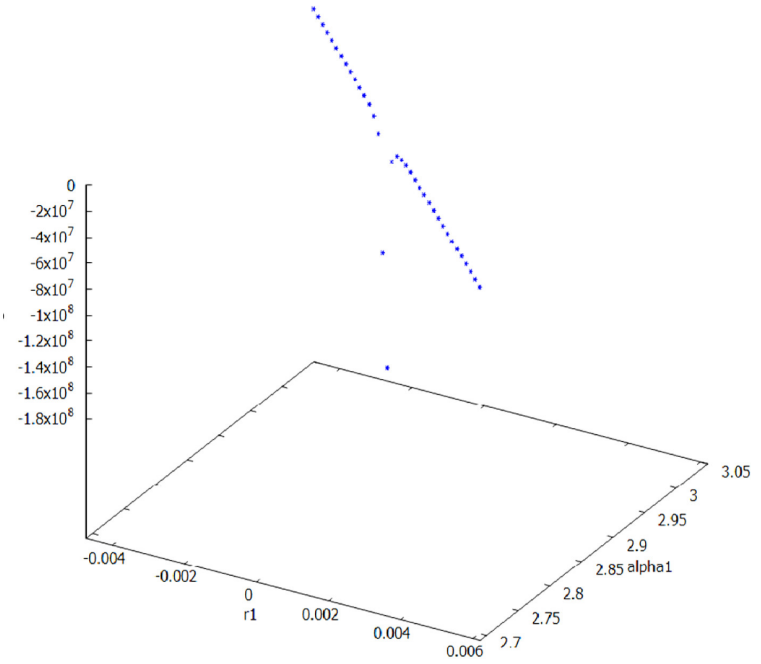

(f) The remaining of the R1212 values

Figure 9: The selected region 4 as the remaining sectional curvature of the R1212 values with $u_1 = \alpha_1$, $u_2 = r_1$, $\theta_1 = \pi/3$ and $\alpha_2 = \pi/3$ for the solution of the nonlinear geodesic differential equations

5.5. The parameters α_2 and r_1

The sectional curvatures of all scenarios, as shown in Fig. 10a and 10b, are each extremely close to zero, indicating that the geometrical manifolds are

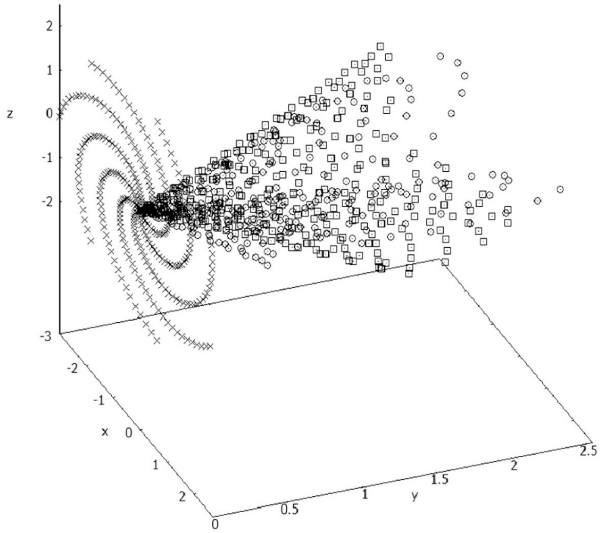

(a) $\theta_1 = \pi$, $\alpha_1 = \pi/6$; $\theta_1 = \pi/4$, $\alpha_1 = \pi/6$; $\theta_1 = \pi/3$, $\alpha_1 = \pi/3$

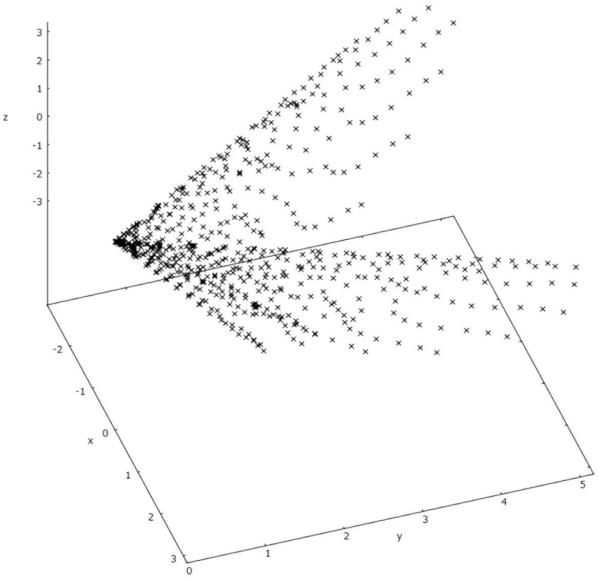

(b) $\theta_1 = \pi/3$ and $\alpha_1 = \pi/3$

Figure 10: The solution of the nonlinear geodesic differential equations for the $u_1 = \alpha_2$, $u_2 = r_1$, $\theta_1 = \pi$ and $\alpha_1 = \pi/6$; $\theta_1 = \pi/4$, and $\alpha_1 = \pi/6$; $\theta_1 = \pi/3$, and $\alpha_1 = \pi/3$

Euclidean flat. The plots of the sectional curvatures are not included because they are all very close to zero. The values range between 10^{-13} to 10^{-9}.

6. Conclusions

The Riemann curvature tensor and geodesic equations are determined for the 1-S robot workspace to realize the path-planning strategies. The results are promising in specifying the path planning with the diffeomorphic and expandable trajectories with the zero and negative sectional curvatures analyzed in the results sections of this paper. The constant negative, positive and zero sectional curvatures can generate hyperbolic, ellipsoid Euclidean geometries, respectively.

The results shows that one needs to choose the convenient parameters of the mechanism for the path planning capabilities. Both the topology of the mechanism, which is 1-S herein, and the parameters of the workspaces should be selected for the pre-defined trajectories of the path planning as shown in the results. The mechanism design and the path planning results are shown to be very much interactively related to each other in this paper. These results will have significant impacts on the research of the self-reconfigurable robots to match the mechanism topology with the path planning capabilities of the selected parameters. Reconfigurable robots have many mechanism topologies to transformed.

Appendix

Homeomorphic spaces are f function, for 1-S robot workspaces, topological spaces that are bijective, continuous, and invertible as f^{-1}. Homeomorphic systems for 1-S robot workspaces are convertible to various manifold shapes using the fiber bundles of path planning via the defined regions of the Riemann sectional curvatures as shown in Fig. A1. Additionally, these are sources of the topological manifold of the homeomorphic group of spaces.

All tangent points structure the tangent bundle T_pM space for the manifolds of the defined 1-S robot workspace. The fiber bundle space is related to the mapping between the differentiable manifolds submersed to structure the whole space. One large spherically shaped manifold can be submersed with the small cylindrically shaped manifolds as the fiber bundle spaces [6]. The tangent bundle generates the isomorphic lines with the vectors for path planning of the 1-S robot workspace via parallel transport.

The topological manifolds select a homeomorphic group of workspaces for path planning of the 1-S robot as shown in Fig. A1.

Figure A1: The path planning strategies for 1-S robot workspace via differential geometry of the Riemann manifold, fibre bundles and tangent bundles

References

[1] J.M. Lee: *Riemannian Manifolds, An Introduction to Curvature*. Springer, 1997.

[2] M.M. Postnikov: *Encyclopedia of Mathematical Sciences*. **91** Geometry VI, Riemannian Geometry. Springer, 2001.

[3] J. Gallier and J. Quaintance: *Differential Geometry and Lie Groups, A Computational Perspective*. Springer, 2020.

[4] S. Hassani: *Mathematical Physics*. Springer, 2013.

[5] H. Sahin: The modular non-overlapping grasp workspaces and dynamics for the grippers using the micro and macro C-manifold design. *Journal of Scientific and Industrial Research*, **80**(9), (2021), 766–776. DOI: 10.56042/jsir.v80i09.47040

[6] L. Godinho and J. Natário: *An Introduction to Riemannian Geometry with Applications to Mechanics and Relativity*. Springer. 2014.

[7] N. Islam: *Tensors and their Applications*. New Age International (P) Ltd., 2006.

[8] Y. Gu: Space-Time Geometry and Some Applications of Clifford Algebra in Physics. *Advances in Applied Clifford Algebras*, **28** (2018), 1–19. DOI: 10.1007/s00006-018-0896-1

[9] E. Marsch and Y. Narita: Connecting in the Dirac Equation the Clifford Algebra of Lorentz Invariance with the Lie Algebra of SU(N) Gauge Symmetry, *Symmetry*, **13**(3), (2021), 475, 1–9. DOI: 10.3390/sym13030475

[10] J. Snygg: *A New Approach to Differential Geometry using Clifford's Geometric Algebra*. Springer, 2012.

[11] M. Gromov and H.B. Lawson: Positive scalar curvature and the Dirac operator on complete Riemannian manifolds. *Publications Mathematiques del'IHES*, **28**(58), (1983), 83–196. DOI: 10.1007/BF02953774

[12] S. Sommer, T. Fletcher, and X. Pennec: Introduction to differential and Riemannian geometry. *Riemannian Geometric Statistics in Medical Image Analysis*, **28** (2020), 3–37, DOI: 10.1016/b978-0-12-814725-2.00008-x

[13] V. Berestovskii and Y. Nikonorov: *Riemannian Manifolds and Homogeneous Geodesics*. Springer, 2020.

[14] H. Sahin: Algorithmic workspace programming of the collaborative multi-robots. *Osmaniye Korkut Ata Üniversitesi Fen Bilimleri Enstitüsü Dergisi*, **5**(1), (2022), 325–341, DOI: 10.47495/okufbed.1030575

[15] H. Sahin: Robot grasping and regrasping kinematics using Lie algebra, the geodesic, and Riemann curvature tensor. *Archives of Control Sciences*, **33**(1), (2023), 5–23, DOI: 10.24425/acs.2023.145111